DOI 10.1007/s11141-015-9617-y
Radiophysics and Quantum Electronics, Vol. 58, No. 6, November, 2015
(Russian Original Vol. 58, No. 6, June, 2015)

INVERSE PROBLEMS OF LOW-FREQUENCY DIAGNOSTICS OF THE EARTH'S CRUST

K. P. Gaikovich[1,3] * **and A. I. Smirnov**[2,3]

UDC 550.837+550.838

We develop and test (in numerical simulation) methods of computer tomography of distributed under-surface inhomogeneities in the conductivity of a medium and for holography (i.e., reconstruction of the shape) of solid and uniformly composed subsurface objects in the context of the problems of multifrequency electromagnetic diagnostics of the Earth's crust structure in the extremely and ultra low frequency bands. The methods are based on solution of the inverse scattering problem using the results provided by multifrequency measurements of the distribution of complex amplitudes of the electromagnetic field on the surface of the medium under consideration.

1. INTRODUCTION

Low-frequency electromagnetic probing of the Earth's crust is performed at frequencies from thousandths to hundreds of hertz using both natural sources (geomagnetic activity) and coherent signals radiated from antennas [1, 2], whose role can be played, in particular, by pipelines and electric power transmission lines. The depth of penetration of electromagnetic waves into the Earth depends on the frequency and can achieve several kilometers in this frequency range, which allows diagnosing. At such depths, the Earth's crust has a layered structure, as a rule, and the frequency spectra of the electric and magnetic fields, which are measured on the Earth's surface, are the initial data for reconstruction of the profile of the geoelectric section (conductivity). This profile is of great interest for solving the problems of geophysics and geology. However, even such a one-dimensional inverse problem is extremely complex. It was formulated for the first time by A. N. Tikhonov in [3], where it was solved for a multilayer medium by the method of minimization of the residual functional. Later, the theory and methods for solving this problem were developed in monograph works [4, 5].

In our works, we continue to develop algorithms intended for solving ill-posed inverse problems and based on mathematically rigorous regularization methods. For example, in [6], the one-dimensional inverse problem of low-frequency probing of the Earth's crust was formulated on the class of continuous functions. We also proposed an algorithm for solving the nonlinear integral equation of the first kind, which was obtained using perturbation theory. In [7, 8], the results of numerical simulation of such a problem were presented on the basis of a specially developed iterative algorithm using Tikhonov's generalized-residual method. However, when simulating strongly contrasting inhomogeneities, this algorithm could result in divergence starting from the second or third iteration. Therefore, in [9] we have started studying the possibilities of the dual-regularization method [10], based on generalization of the Lagrangian approach to the optimization theory, which is new in the theory of nonlinear ill-posed inverse problems. Its efficiency was demonstrated by numerical simulation [11].

* gai@ipm.sci-nnov.ru

[1] Institute for Physics of Microstructures of the Russian Academy of Sciences; [2] Institute of Applied Physics of the Russian Academy of Sciences; [3] N. I. Lobachevsky State University of Nizhny Novgorod, Nizhny Novgorod, Russia. Translated from Izvestiya Vysshikh Uchebnykh Zavedenii, Radiofizika, Vol. 58, No. 6, pp. 476–491, June 2015. Original article submitted September 16, 2014; accepted February 1, 2015.

Fast development of computational tools allowed one to apply the concepts of multifrequency electromagnetic probing of the Earth's crust for diagnostics of three-dimensional (volume) inhomogeneities of conductivity on the basis of the data of multifrequency two-dimensional scanning of the scattered electromagnetic field over the Earth's surface. The methods of retrieving the parameters of such inhomogeneities (computer tomography techniques) were developed with the use of various approaches to solving the inverse scattering problem formulated within the framework of three-dimensional integral equations of perturbation theory for the electromagnetic field (see monograph work [12]). In this case, use was made of reduction of these equations to a simpler system with the subsequent regularization following Tikhonov's technique [13, 14], parametrization [15], and the statistical [16] and neural network [17] approaches.

The complexity of solving three-dimensional nonlinear ill-posed inverse problems consists in fundamental limitations imposed on the dimension of discretization of the algorithms and, consequently, on the achievable resolving power. For example, when we specify the dimension equal to 100 elements along each coordinate, we find that for the six-dimensional kernel of the three-dimensional equation solved, it is necessary to store 10^{12} numbers in the computer memory, which makes the use of supercomputers necessary. This is why all the above-cited works employ various simplifying approximations, use parametrization and modeling, which reduce the dimension of the desired distribution, introduce (from various considerations) first approximations close to the solution, and apply the methods which does not have sufficient justification.

The limitations imposed on the dimension of discretization can be overcome using the approach [18, 19] developed by us and based on reduction of three-dimensional integral equations to equations of the convolution type with respect to the transverse coordinates. This allows one to use the two-dimensional Fourier transform in order to reduce the problem to multiple solution of the one-dimensional integral Fredholm equation of the first kind for each pair of components of the transverse spectrum in the wave-vector space. It was shown in [8, 18, 19] that the proposed simplification is possible in cases where the probing field is a locally plane wave, which, in particular, takes place in the problem of geomagnetic probing, as well as when scanning by a rigidly coupled transmitter–receiver system. We implemented this scheme as a method of near-field multifrequency tomography in the microwave band [20]. The efficiency of this method was demonstrated experimentally in the case of dielectric inhomogeneities in the ground, which were located in the near zone of the antenna system. In [20, 21], a method of visualization of this surface was developed for internally homogeneous objects, which are determined completely by the shape of their surfaces, i.e., the problem of computer holography was solved.

In this work, we use the experience accumulated in the process of solving the problems of subsurface microwave probing as a basis for the development of algorithms of multifrequency tomography and holography of three-dimensional inhomogeneities of conductivity of the Earth's crust in extremely low-frequency (ELF) and ultra low-frequency (ULF) bands. Additionally, the method of selection of the fields scattered by surface and subsurface inhomogeneities, which was proposed in [20], is generalized to the case of strongly conducting media by means of converting the data of measurements at various frequencies to a specially synthesized pseudopulse. The performed numerical simulation clearly demonstrates the efficiency of the methods used for solving the inverse problem of low-frequency diagnostics of the Earth's crust.

2. TOMOGRAPHY AND HOLOGRAPHY OF LOW-CONTRAST THREE-DIMENSIONAL INHOMOGENEITIES OF CONDUCTIVITY OF THE EARTH'S CRUST

Let a given current source with the density $\mathbf{j}(\mathbf{r})\exp(-i\omega t)$, where $\mathbf{r}$ is the radius vector, t is the time, and ω is the angular frequency, be located in free space ($z > 0$) over the half-space $z < 0$ filled with a medium having the complex dielectric permittivity $\varepsilon_- = \varepsilon_0 + \varepsilon_1(\mathbf{r})$. The z axis of the Cartesian coordinate system (x, y, z) is directed upwards with the point $z = 0$ corresponding to the interface of the medium and free space, and the x and y axes are directed along this interface. The electromagnetic field excited by such a source satisfies the Maxwell equations

$$\operatorname{rot}\mathbf{E} = \frac{i\omega}{c}\mathbf{H}, \tag{1}$$

$$\operatorname{rot}\mathbf{H} + \frac{i\omega}{c}[\bar{\varepsilon}(z) + \varepsilon_1(\mathbf{r})]\,\mathbf{E} = \frac{4\pi}{c}\mathbf{j}(\mathbf{r}), \tag{2}$$

where $\mathbf{E}$ and $\mathbf{H}$ are the complex amplitudes of the electric and magnetic fields, c is the speed of light in free space, $\varepsilon_1 = 0$ and $\bar{\varepsilon} = 1$ for $z > 0$, and the current density $\mathbf{j} = 0$ and $\bar{\varepsilon} = \varepsilon_0$ for $z < 0$.

We transpose the term proportional to $\varepsilon_1(\mathbf{r})$ to the right-hand side and consider it as an effective source of the scattered radiation with the current density $\mathbf{j}_{\text{eff}} = -i\omega\varepsilon_1(\mathbf{r})\mathbf{E}/(4\pi)$:

$$\operatorname{rot}\mathbf{H} + \frac{i\omega}{c}\bar{\varepsilon}(z)\mathbf{E} = -\frac{i\omega}{c}\varepsilon_1\mathbf{E} + \frac{4\pi}{c}\mathbf{j} = \frac{4\pi}{c}(\mathbf{j}_{\text{eff}} + \mathbf{j}). \tag{3}$$

Using the formalism of the Green's functions calculated for the medium with the dielectric permittivity $\bar{\varepsilon}(z)$, one can write the integral formulas, which relate the electric field $\mathbf{E}^{(1)}(\mathbf{r}) = \mathbf{E}(\mathbf{r})$ in free space for $z > 0$ and the electric field $\mathbf{E}^{(2)}(\mathbf{r}) = \mathbf{E}(\mathbf{r})in the medium$ for $z < 0$ [19]:

$$\begin{aligned} E_i^{(1)}(\mathbf{r}) &= E_{0i}^{(1)}(\mathbf{r}) + E_{1i}^{(1)}(\mathbf{r}) = E_{0i}^{(1)}(\mathbf{r}) - \frac{i\omega}{4\pi}\int\limits_{V'} \varepsilon_1(\mathbf{r}')E_j^{(2)}(\mathbf{r}')G_{ji}^{21}(x-x', y-y', z, z')\,\mathrm{d}^3r', \\ E_i^{(2)}(\mathbf{r}) &= E_{0i}^{(2)}(\mathbf{r}) + E_{1i}^{(2)}(\mathbf{r}) = E_{0i}^{(2)}(\mathbf{r}) - \frac{i\omega}{4\pi}\int\limits_{V'} \varepsilon_1(\mathbf{r}')E_j^{(2)}(\mathbf{r}')G_{ji}^{22}(x-x', y-y', z, z')\,\mathrm{d}^3r', \end{aligned} \tag{4}$$

where

$$\begin{aligned} E_{0i}^{(2)}(\mathbf{r}) &= \int\limits_{V'} j_j(\mathbf{r}')G_{ji}^{12}(x-x', y-y', z, z')\,\mathrm{d}^3r', \\ E_{0i}^{(1)}(\mathbf{r}) &= -\frac{i\omega}{4\pi}\int\limits_{V'} j_j(\mathbf{r}')G_{ji}^{11}(x-x', y-y', z, z')\,\mathrm{d}^3r'. \end{aligned} \tag{5}$$

Here, we imply summation over the repeated indices i and j, which stand for x, y, or z, $G_{ji}^{kl}(x-x', y-y', z, z')$ are the elements of the tensor Green's function, each of which is equal to the value of the ith projection of the electric field produced at the point $\mathbf{r} = (x, y, z)$ in the medium with the dielectric permittivity $\bar{\varepsilon}(z)$ by the jth component of the current density $j_j \propto \delta(\mathbf{r} - \mathbf{r}')$ of a given point source, and the superscripts k and l take two values and identify the media in which the source and the source-excited field are considered (the half-spaces $z > 0$ and $z < 0$ correspond to 1, to 2, respectively). The fields $\mathbf{E}_1^{(1)}(\mathbf{r})$ and $\mathbf{E}_1^{(2)}(\mathbf{r})$ are the scattered fields in media 1 and 2, respectively.

Equations (5) determine the structure of the unperturbed probing fields $\mathbf{E}_0^{(1)}(\mathbf{r})$ and $\mathbf{E}_0^{(2)}(\mathbf{r})$, which correspond to the given distribution of the current density $\mathbf{j}(\mathbf{r})$. We are interested in the inverse problem of reconstruction of the inhomogeneous correction $\varepsilon_1(\mathbf{r})$ to the dielectric permittivity on the basis of the scattered field $\mathbf{E}_1^{(1)}(\mathbf{r})$ in free space, which is equal, according to Eq. (4), to

$$E_{1i}^{(1)}(\mathbf{r}) = -\frac{i\omega}{4\pi}\int\limits_{V'} \varepsilon_1(\mathbf{r}')E_j^{(2)}(\mathbf{r}')G_{ji}^{21}(x-x', y-y', z, z')\,\mathrm{d}^3r'. \tag{6}$$

In this case, as well as in [18–20], we assume that the multifrequency-measurement data for the transverse distributions of the scattered-field components $E_{1i}^{(1)}(x, y, z_0, \omega)$ in the plane $z = z_0 > 0$ over the surface of the probed medium are known.

It is natural to start solving problem (6) with the so-called Born approximation, where the unper-

turbed probing field $E_{0j}^{(2)}$ from Eq. (5) is substituted into the integral instead of $E_j^{(2)}$:

$$E_{1i}^{(1)}(x,y,z_0,\omega) = -\frac{i\omega}{4\pi}\int\limits_{V'} \varepsilon_1(\mathbf{r}',\omega)E_{0j}^{(2)}(\mathbf{r}',\omega)G_{ji}^{21}(x-x',y-y',z_0,z',\omega)\,\mathrm{d}^3r'. \tag{7}$$

As has already been noted, the numerical solution of this three-dimensional problem has major limitations imposed on the discretization dimension and, consequently, on the achievable resolving power. In [17, 19], methods for reducing integral equation (7) to the convolution with respect to the transverse coordinates were proposed. One of such methods is based on the assumption that the probing field is a plane wave. In a medium, this field is decomposed into a sum of the components

$${}^{\alpha}E_{0i}^{(2)}(\mathbf{r}') = {}^{\alpha}E_{0i}^{(2)\,\alpha}T^{12}(\kappa_x,\kappa_y)\exp\Big(i\kappa_x x' + i\kappa_y y' - i\sqrt{k^2-\kappa_\perp^2}\,z'\Big), \tag{8}$$

with the electric-field polarization parallel and perpendicular to the incidence plane, where ${}^{\alpha}T^{12}$ are the coefficients of wave transmission from free space to the medium with the parallel ($\alpha = \|$) and perpendicular ($\alpha = \perp$) polarizations [19], $k = \omega\sqrt{\varepsilon_0}/c$, and ${}^{\alpha}E_{0i}$ is the value of the unperturbed field projected in the axis i at the origin of coordinates.

Using the formula for the convolution of the product of the function and the exponential, from Eq. (6) we obtain the following one-dimensional equation for the depth profile of the transverse inhomogeneity spectrum:

$$E_{1i}^{(2)}(k_x,k_y,z_0,\omega) = -i\pi\omega\int\limits_{z'} \varepsilon_1(k_x-\kappa_x,k_y-\kappa_y,z',\omega)E_{0j}^{(2)}(\kappa_x,\kappa_y,z',\omega)G_{ji}^{21}(k_x,k_y,z_0,z',\omega)\,\mathrm{d}z', \tag{9}$$

where the elements of the tensor Green's function in the wave-vector space (k-space) are obtained in explicit form for an arbitrary multilayer medium by expanding the source field in terms of plane waves using the formalism of the input impedance method [19]. Hereafter, for brevity we use the same notations for the transverse spectra as for the functions themselves with few exceptions. The functions are identified by the corresponding arguments. Multiple solution of Eq. (9) for each pair (k_x, k_y) yields the solution of the problem in the k-space, wherefrom the desired three-dimensional distribution $\varepsilon_1(x,y,z,\omega)$ is found by means of the inverse Fourier transform.

The above-described situation takes place in the case of geomagnetic ELF and ULF probing of the Earth's crust with the use of the field of remote natural sources. Then, the Leontovich impedance boundary conditions for low-frequency radio waves are fulfilled, and we can assume that the probing field in the conducting medium is a locally plane wave propagating into the Earth along the normal to its surface, while the Earth's crust is a conductor with the purely imaginary permittivity $\varepsilon = \varepsilon' + i\varepsilon'' \approx 4\pi i\sigma_0/\omega$, which is determined by the conductivity σ_0. In the case of a homogeneous medium, the exact solution of the Maxwell equations with the boundary conditions

$$E_x(z=0,\omega) = E_{0y}(\omega), \qquad H_y(z=0,\omega) = H_{0y}(\omega) \tag{10}$$

on the surface $z = 0$ has the form

$$E_x(\omega,z) = E_{0x}(\omega)\exp(z/\delta - iz/\delta), \tag{11}$$

$$H_y(\omega,z) = -\frac{c\,(i+1)}{\omega\delta}E_x(\omega,z) = -\frac{1}{Z}E_x(\omega,z) = H_{0y}(\omega)\exp(z/\delta - iz/\delta), \tag{12}$$

where $\delta = c/\sqrt{2\pi\omega\sigma_0}$ is the skin depth and Z is the impedance of the medium, which is determined by its conductivity in the case of a homogeneous medium. A deviation of the impedance off the value calculated for the surface conductivity indicates the presence of a subsurface inhomogeneity and is an

input parameter in most methods of geomagnetic probing of one-dimensionally inhomogeneous geological structures. Equations (11) and (12) are also used to solve integral equations (4) and (7) in the Born approximation.

If the variations in the electric-field component E_x on the ground surface ($z = 0$) as functions of the incident-wave frequency in the ULF band are measured by the method of two-dimensional scanning, then, under the fulfillment of the Leontovich boundary conditions, integral equation (9) for the problem of tomography of the Earth's crust conductivity is written in the Born approximation as

$$E_{1x}(\kappa_x, \kappa_y, \omega) = \frac{E_{0x}}{2i\sigma_0} \frac{\kappa_z \kappa_x^2 {}^{\parallel}T^{21} + \kappa_y^2 k^{2\perp} T^{21}/\kappa_z}{\kappa_\perp^2} \int\limits_{-\infty}^{0} \sigma_1(\kappa_x, \kappa_y, z') \exp\Big(\frac{z'}{\delta} - \frac{iz'}{\delta}\Big) \exp\Big(-i\sqrt{k^2 - \kappa_\perp^2}\, z'\Big)\, \mathrm{d}z', \quad (13)$$

where $\sigma_1(\kappa_x, \kappa_y, z')$ is the depth profile of the transverse spectrum of the conductivity inhomogeneity, and ${}^{\alpha}T^{21}$ stands for the coefficients of transmission of the electromagnetic field from the medium to free space for the parallel ($\alpha = \parallel$) and perpendicular ($\alpha = \perp$) polarizations.

A similar equation is written for the y-component H_{1y} of the magnetic field:

$$H_{1y}(\kappa_x, \kappa_y, \omega) = H_{0y} \frac{\kappa_x^2 {}^{\parallel}T^{21} + \kappa_y^2 {}^{\perp}T^{21}}{\kappa_\perp^2} \frac{(1+i)\,\omega\delta}{c^2} \int\limits_{-\infty}^{0} \sigma_1(\kappa_x, \kappa_y, z') \exp\Big(\frac{z'}{\delta} - \frac{iz'}{\delta}\Big) \exp\Big(-i\sqrt{k^2 - \kappa_\perp^2}\, z'\Big)\, \mathrm{d}z'. \quad (14)$$

Equations (13) and (14) are Fredholm equations of the first kind for the depth distribution of the transverse spectral components of the conductivity inhomogeneity. One can see that the contribution of the medium inhomogeneities to the field perturbation decreases exponentially on the skin depth δ, whose value depends on the frequency and increases with decreasing frequency. This fact is the basis for the method of deep ULF probing. At the same time, the integrand in Eqs. (13) and (14) contains another term, which decays exponentially as the depth of penetration into the medium increases. This term manifests itself for great transverse wave numbers and is related to the near-zone components of the transverse spectrum of the scattered field.

For probing with the use of artificial sources of the probing field, three-dimensional equation (7) in the general case ceases to be a convolution-type equation and cannot be reduced to one-dimensional equation (9). However, it was shown in [19] that for the measurement scheme employing the rigidly connected transmitter—receiver system, in which the distance between the transmitter and receiver is specified by the vector $\delta\mathbf{r} = (\delta x, \delta y, \delta z)$, the integral equation for the electromagnetic field in the Born approximation also has the form of a convolution with respect to the transverse coordinates x and y. This allows one to obtain a one-dimensional integral equation for each pair of the components k_x and k_y of the transverse spectrum of the scattered field by using the two-dimensional Fourier transform. This approach was implemented experimentally as the method of subsurface microwave near-field tomography of inhomogeneities in the ground [20]. It can also be generalized to the case of low-frequency probing of the Earth's crust, where the corresponding integral equation for the electric field has the form

$$E_{1i}(k_x, k_y, z_0, \omega, z, \delta\mathbf{r}) = 16\pi^4 \int\limits_{z'} \sigma_1(k_x, k_y, z') \iint\limits_{-\infty}^{+\infty} \exp(-\kappa_x \delta x - \kappa_y \delta y) \int\limits_{z'} \big[j_i(\kappa_x, \kappa_y, z'' - z - \delta z, \omega) \times G_{ij}^{12}(\kappa_x, \kappa_y, z'', z', \omega)\big] G_{ji}^{21}(\kappa_x + k_x, \kappa_y + k_y, z', z, \omega)\, \mathrm{d}\kappa_x\, \mathrm{d}\kappa_y\, \mathrm{d}z''\, \mathrm{d}z'. \quad (15)$$

In such a formulation, the probing field is strongly localized near the source, which ensures a better

resolving power. However, it is difficult to develop scanning systems for sources having large sizes. For example, the power transmission lines and pipelines, which are commonly used as low-frequency antennas, are certainly unsuitable for this purpose. Therefore, the above-described approach can be used only for probing subsurface inhomogeneities at relatively small depths.

Herein, when considering the problem of electromagnetic diagnostics of the Earth's crust, we study thoroughly the method based on solving of Eq. (14) using the data of multifrequency measurements of the magnetic field, which significantly exceeds the electric field near the conducting surface.

Let us represent first-kind Fredholm equation (14) in concise form as

$$H(k_x, k_y, \omega) = \int\limits_{z'} \sigma_1(k_x, k_y, z') K(k_x, k_y, z', \omega)\, \mathrm{d}z', \tag{16}$$

where $K(k_x, k_y, z', \omega)$ is the equation kernel.

Theoretically, it is quite possible to solve the inverse problem on the basis of this equation. However, the experience of using a similar equation for the subsurface diagnostics in the microwave band [20] showed that the useful signal from a subsurface object is poorly discernible against the background of noise due to scattering from subsurface inhomogeneities. This difficulty was overcome by transforming multifrequency data to a synthesized complex pseudopulse, in which the uncorrelated noise error and the useful signal were isolated effectively, and this signal acquired depth selectivity:

$$H_1(x, y, t) = \int\limits_{\Delta\omega} H_1(x, y, \omega) \exp(i\omega t)\, \mathrm{d}\omega, \tag{17}$$

where $\Delta\omega$ is the analyzed frequency band. In Eq. (17), it is convenient to pass from the time parameter to the parameter z_s of the effective depth of the scattering element (allowing for the velocity of propagation in the medium along the path to the scattering element and back) according to the relation

$$H_1(x, k_y, z', z_\mathrm{s}) = H_1[k_x, k_y, z', z_\mathrm{s} = -ct/(2\,\mathrm{Re}\sqrt{\varepsilon_0})]. \tag{18}$$

Unlike the actual pulse, the quantity (pseudopulse) introduced in [20] is complex-valued and described by an integral over a limited frequency range $\Delta\omega$. At the same time, the pseudopulse preserves such an important property of the actual pulse as the distance selectivity (or depth selectivity, in this case). It clearly indicates the position of the surface, as well as the contribution of the probed object in a certain range of the values of z_s. This property allows one to localize and visualize the region of scattering from the object in the coordinates (x, y, z_s). Such a region is evidently wider than the object itself and has blurred boundaries, but the average depth of the object along the z coordinate corresponds approximately to the position of the visualized psedopulse along z_s. Information obtained by simple preprocessing of the measurement data allows one to radically decrease the region in which the solution to the problem is found, which is of critical importance for solving ill-posed equations of the considered type [19].

To use the above-mentioned advantages, one should employ the transformed equation, which relates the depth profile of the transverse spectrum of the inhomogeneity and the transverse spectrum of the complex pseudopulse and which preserves its type. In that equation, only the kernel is transformed:

$$H(k_x, k_y, z_\mathrm{s}) = \int\limits_{z'} \sigma_1(k_x, k_y, z') K_1(k_x, k_y, z', z_\mathrm{s})\, \mathrm{d}z', \tag{19}$$

$$K_1(k_x, k_y, z', z_\mathrm{s}) = \int\limits_{\Delta\omega} K(k_x, k_y, z', \omega) \exp(-2i\omega z_\mathrm{s}\, \mathrm{Re}\sqrt{\varepsilon_0}/c)\, \mathrm{d}\omega. \tag{20}$$

The solution for each pair of the components in the transverse spectrum of the conductivity inhomogeneity is found using the algorithm [19], which is based on Tikhonov's generalized-residual method for complex-

valued functions in Sobolev's Hilbert space W_2^1. Then, using the inverse Fourier transform in the k-space to solve Eq. (19), we find the desired three-dimensional distribution

$$\sigma_1(x,y,z) = \iint \sigma_1(k_x,k_y,z)\exp(ik_x x + ik_y y)\,\mathrm{d}k_x\,\mathrm{d}k_y. \tag{21}$$

One can visualize this distribution in the section by an arbitrary plane, i.e., perform tomographic analysis.

Since the conductivity of the Earth's crust lies in a wide range, 10^{-5}–10^{-1} S/m, the frequency range $\Delta\omega$ for solving inverse problem (19) should be chosen with allowance for the estimate of the skin depth δ corresponding to the assumed probing depth. For example, tomography of inhomogeneities at depths from 0.2 up to 5–7 km requires the fulfillment of the condition $0.1 < \delta < 10$ km, which requires measurements in the frequency range $0.25 < f < 2500$ for the conductivity $\sigma_0 = 10^{-2}$ S/m, and in the range $12 < f < 125000$ Hz $\sigma_0 = 2\cdot 10^{-4}$ S/m for $\sigma_0 = 2\cdot 10^{-4}$ S/m.

2.1. Tomography of distributed inhomogeneities

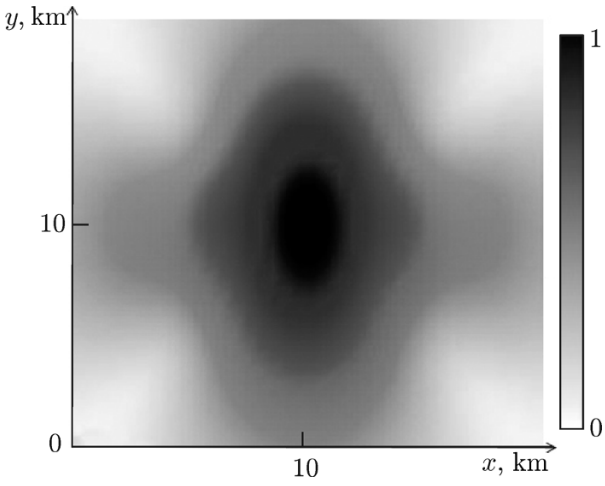

Fig. 1. Distribution of the normalized pseudopulse amplitude $|H_{1y}(x,y,z_\mathrm{s} = -4\ \mathrm{km})|/H_{\max}$.

We have developed an algorithm for numerical implementation of the method of computer tomography of subsurface inhomogeneities, i.e., reconstruction of the three-dimensional distribution $\sigma_1(x,y,z)$ of the conductivity inhomogeneity in the probed medium, which is based on solving Eq. (19), and then performed the corresponding numerical simulation. As the initial data for analysis, we used multifrequency "measurements" of the distribution of the complex amplitudes $H_{1y}(x,y,\omega)$ of the scattered field in the two-dimensional region over the surface of the medium with the inhomogeneity. To use these data in Eq. (19), their frequency dependence was transformed to the transverse spectrum of the synthesized pseudopulse $H_{1y}(x,y,z_\mathrm{s})$.

Figure 1 shows the transverse distribution of the pseudopulse amplitude, normalized to the maximum amplitude $H_{\max}$, for the Gaussian conductivity inhomogeneity $\sigma_1(x,y,z) = \sigma_1^0\exp[-(x-x_\mathrm{t})^2/\Delta x^2 - (y-y_\mathrm{t})^2/\Delta y^2 - (z-z_\mathrm{t})^2/\Delta z^2]$, which has the parameters $\Delta x = 2$ km, $\Delta y = 3$ km, and $\Delta z = 1$ km, and is located at the depth $z_\mathrm{t} = -3.5$ km in a medium with the conductivity $\sigma_1^0 = 0.01$ S/m.

The numerical simulation based on solving Eq. (19) was performed following a closed-loop scheme: the two-dimensional distribution of the scattered field near the medium surface was calculated at frequencies of the chosen range for the specified inhomogeneity, a normally distributed random "measurement error" with a given variance was added, the initial data (transverse spectrum of the pseudopulse) were calculated in Eq. (19), Tikhonov's method was used to solve the inverse problem for each pair of the spectral components, and inverse Fourier transform (21) was used to calculate the desired three-dimensional distribution of the conductivity inhomogeneity, which was compared with the initial distribution. In the tomography results, which are presented in what follows, high-quality reconstruction was ensured by the random-error level 10% in the integral metric, and the result depended only weakly on the error-level variations within the limits ±5%.

As an example, we demonstrate the advantage of converting the frequency spectrum of the signal to a synthesized pseudopulse for the above-described Gaussian inhomogeneity. Figure 2 shows the transverse distributions (along the x axis in the section $y = y_\mathrm{t}$) of the frequency dependence of the field incident on the surface for two values of the inhomogeneity depth, $z_\mathrm{t} = -3.5$ and -7 km.

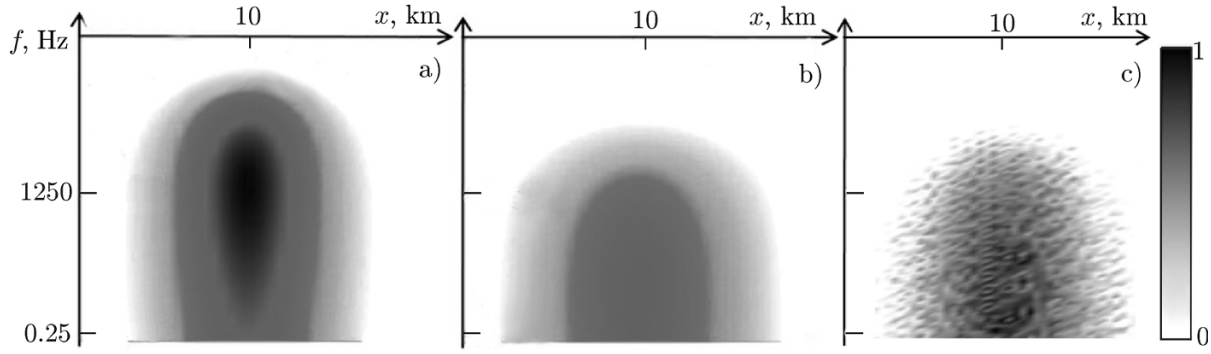

Fig. 2. Distribution of the normalized amplitude $|H_{1y}(x, y, y_t, f)|/H_{max}$ of the scattered field for a Gaussian inhomogoneity located at the depths $z_t = -3.5$ km, $z_t = -7$ km, and $z_t = -7$ km with an introduced arbitrary error (*a*, *b*, and *c*, respectively).

One can see that as the frequency decreases, the inhomogeneity located closer to the surface (at $z_t = -3.5$ km) starts manifesting itself in the signal earlier than that located deeper (at $z_t = -7$ km), and the signal received from the latter is significantly weaker. Evidently, it is difficult to make judgements on depth localization of the probed object on the basis of these distributions.

Figure 3 shows the distribution of the pseudopulse amplitude over the coordinates (x, z_s) in the section $y = y_t$. It demonstrates the possibility of approximate localization of the depth location of inhomogeneities. The positions of the pseudopulse maxima on the axis of the effective scattering depth z_s correspond approximately to the depths z_t of the probed inhomogeneities. Such visualization allows one to choose informative intervals Δx, Δy, and Δz_s, which determine the region of the pseudopulse quantities used for analysis, as well as the intervals Δx, Δy, and $\Delta z = \Delta z_s$, which determine the region where the solution is sought. These data represent rather important *a priori* information for solving the ill-posed problem under consideration.

Figure 4 shows the numerical simulation results for the solution of the inverse problem, which was found following the closed-loop scheme for the above-described Gaussian inhomogeneity at the depths $z_t = -3.5$ and -7 km in the vertical section $y = y_t$. The reconstructed distributions were obtained using inverse Fourier transform (21) of the solution of inverse problem (19). The results are presented in the form normalized to the maximum ($\sigma_1^0 = 1$).

One can see that the shapes and positions of the reconstructed inhomogeneities correspond well to the simulated distributions. For the inhomogeneity at a depth of -3.5 km, the maximum error of the conductivity value amounts to about 10%, and for the inhomogeneity at a depth -7 km, it is about 20%. One can also see that as the depth increases, the reconstructed distribution becomes blurred, which is quite natural for the ill-posed problem solved. Figure 5 shows the results of tomography in the horizontal cross section $z = z_t$ at the depth $z_t = -3.5$ km.

2.2. Holography of continuous inhomogeneities

Since in practice most inhomogeneities have an internally homogeneous structure, a topical task is to solve the problem of reconstructing the shape of the surfaces of such inhomogeneities. This allows visualizing the inhomogeneity at any aspect to the observer, i.e., solving the problem of computer holography. To do this, it is necessary to supplement the algorithm with additional *a priori* information on invariance of dielectric parameters inside the diagnosed object. Here, one can use the approach which we developed in [20, 21] for simply connected objects in the context of microwave probing. This approach employs directly the profile of the transverse spectrum inhomogeneity in the k-space, which was reconstructed from the solution of Eq. (19).

In the Cartesian coordinate system bound to the medium surface, we specify the shape of the surface of a homogeneous object ($\sigma_1 = \sigma_1^0 = \text{const}$) using the functions $x_1(y, z)$ and $x_2(y, z)$ (see Fig. 6*a*). Then, for the inverse Fourier transform of this spectrum with respect to k_y, we have an equation which is equivalent

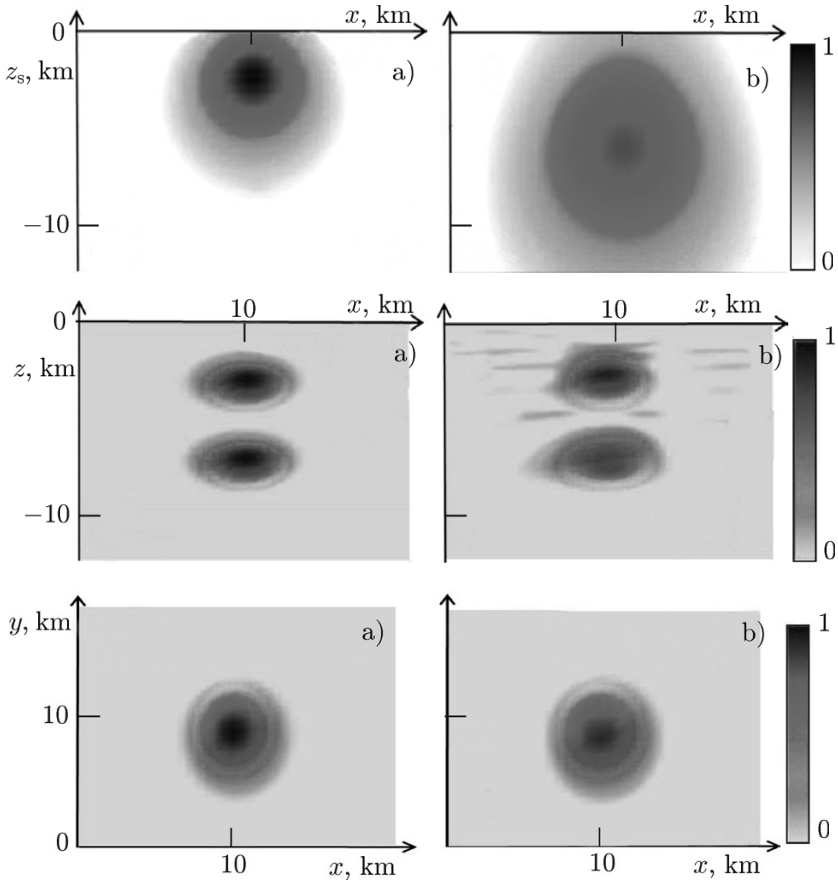

Fig. 3. Distribution of the normalized amplitude $|H_{1y}(x, y = y_t, f)|/H_{\max}$ for the Gaussian inhomogeneity located at the depths $z_t = -3.5$ km (*a*) and $z_t = -7$ km (*b*).

Fig. 4. Simulated (*a*) and reconstructed (*b*) distributions of the Gaussian inhomogeneities of conductivity (vertical sections through their centers).

Fig. 5. Simulated and reconstructed (*a* and *b*, respectively) distributions of the Gaussian conductivity inhomogeneities (horizontal cross sections through their centers).

to the system of two equations for its real and imaginary parts:

$$\sigma_1(k_x, y, z) = \frac{\sigma_1^0}{2\pi i k_x}\Big\{\exp[-ik_x x_1(y,z)] - \exp[-ik_x x_2(y,z)]\Big\}. \tag{22}$$

Solution of this equations yields the functions $x_1(y, z)$ and $x_2(y, z)$ which determine the desired shape of the object surface. In principle, this equation is solvable for any value of k_x and is overdetermined. Numerical simulation shows that the best results are obtained when choosing $k_x \approx 2\pi/L$, where L is the estimate of the transverse size of the inhomogeneity on the basis of the visualized image of the pseudopulse.

This approach can be generalized to the case where the object contains a simply connected inclusion with the conductivity $\sigma_1 = \sigma_1^{02} = \text{const}$. When seeking the shape of the inclusion specified by the functions $x_3(y, z)$ and $x_4(y, z)$ in each section $z = \text{const}$, as is shown in Fig. 6*b*, we obtain a system of complex equations for two or more values of k_x:

$$\sigma_1(k_x, y, z) = \frac{\sigma_1^0}{2\pi i k_x}\Big\{\exp[-ik_x x_1(y,z)] - \exp[-ik_x x_2(y,z)]\Big\} + \frac{\sigma_1^{02} - \sigma_1^0}{2\pi i k_x}\Big\{\exp[-ik_x x_3(y,z)] - \exp[-ik_x x_4(y,z)]\Big\}. \tag{23}$$

It should be noted that the results of tomographic analysis cannot be used directly to find the boundaries of a continuous object. This is due both to blurring of sharp details in the process of solving an ill-posed problem with allowance for the data error, and to fundamental limitations related to the fact that for functions with jumps, Dini's test for pointwise convergence of Fourier series, which represent numerical solution (21), is violated. This leads to a distortion of the result due to the Gibbs effect. The proposed approach is a consistent solution of the problem under consideration.

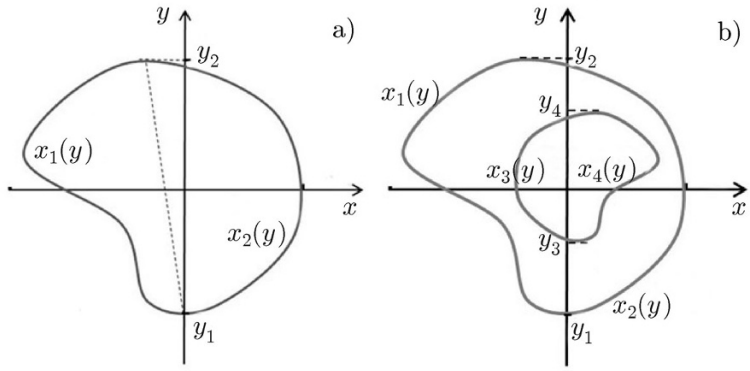

Fig. 6. Sections $z' = \text{const}$ of a continuous object (*a*) and an object with an inclusion (*b*).

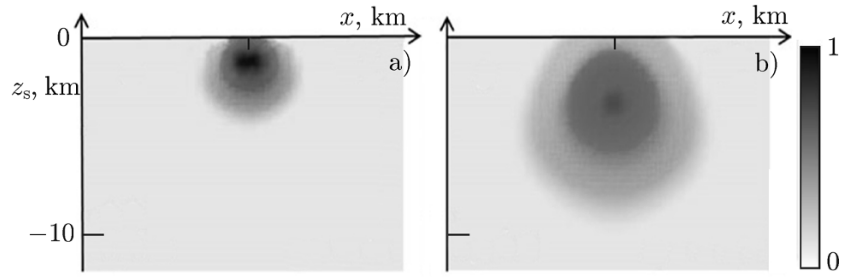

Fig. 7. Distributions of the normalized amplitude $|H_{1y}(x, y = 10\ \text{km}, z_s)|/H_{\max}$ of the pseudopulse of the scattered field for the Gaussian inhomogeneity located at the depths $z_t = -2$ km (*a*) and $z_t = -4.5$ km (*b*).

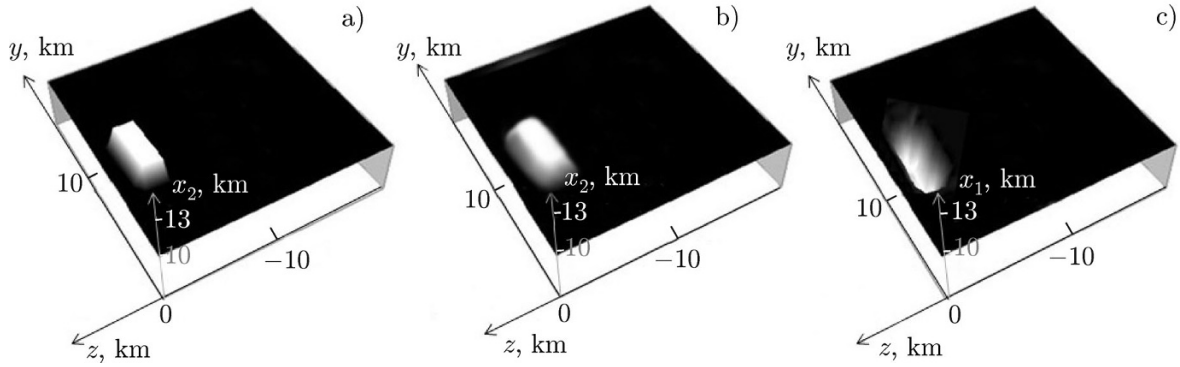

Fig. 8. Shape of the simulated inhomogeneity of conductivity at the depth $z_t = -2$ km (the part specified by the function $x_2(y, z)$ by analogy with Fig. 6*a*) (*a*) and the corresponding results of the holographic analysis in the form of the functions $x_2(y, z)$ (*b*) and $x_1(y, z)$ (*c*).

In what follows, we present the results of numerical simulation of the "holographic" method for an inhomogeneity shaped as a parallelepiped with dimensions of $4 \times 4 \times 2$ km, which is located at the depths $z_t = -2$ km and -4.5 km.

Figure 7 shows the distributions of the amplitudes of the scattered-field pseudopulse. One can see that the positions of the pseudopulse maxima along the axis of the effective scattering depth z_s correspond approximately to the depths of the probed inhomogeneities. Figures 8 and 9 present the results of holographic analysis, i.e., the object shape found by solving Eq. (22) and specified in the form of two functions, as is shown in Fig. 6*a*. It is seen that the reconstructed shape of the object at the depth $z_t = -2$ km reproduces the shape of the initial parallelepiped recognizably and corresponds well to its position and dimensions. In the case of a greater depth of the object (Fig. 9), its contours are blurred, but, on the whole, the reconstructed shape agrees well with the shape, position, and dimensions of the simulated object.

Comparing the results of the holographic analysis, which are presented in Figs. 8 and 9, with the results of near-field holography at microwave frequencies [20, 21], one can easily see that in the case considered here, it is much more difficult to achieve a comparable resolving power (on the scale of wavelengths in the medium). This is related to the use of a localized source, rather than a plane wave, in the process of microwave field probing.

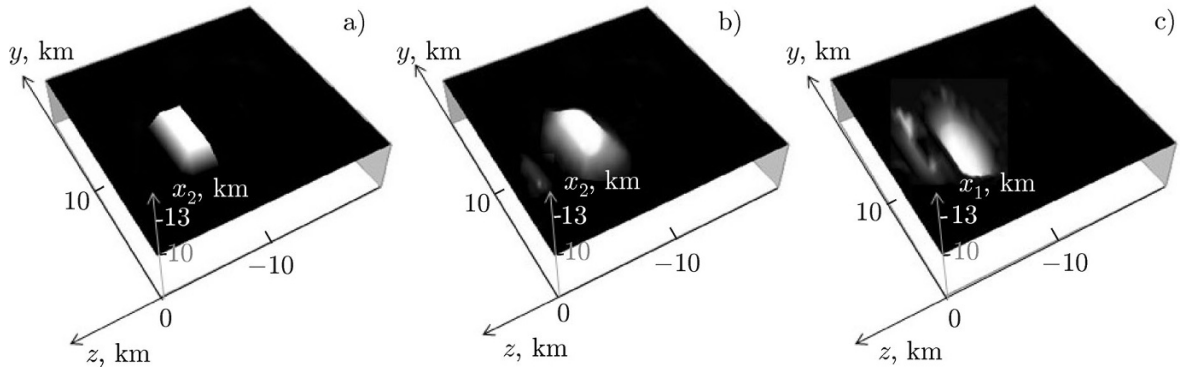

Fig. 9. Shape of the simulated inhomogeneity of conductivity at the depth $z_t = -4.5$ km (the part specified by the function $x_2(y, z)$) (*a*) and the corresponding results of the holographic analysis in the form of the functions $x_2(y, z)$ (*b*) and $x_1(y, z)$ (*c*).

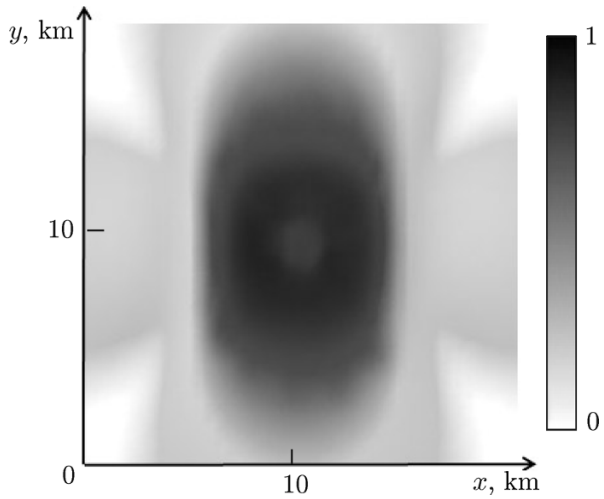

Fig. 10. Transverse distribution of the normalized pseudopulse amplitude $|H_{1y}(x, y, z_s = -2 \text{ km})|/H_{max}$.

Figure 10 shows the transverse distribution of the pseudopulse for the object having the same shape as in Fig. 1, dimensions of $4 \times 4 \times 3$ km, and a cavity with dimensions of $2 \times 2 \times 1.5$ km for $\sigma_0 = 5 \cdot 10^{-4}$ S/m, $\sigma_1^0 = 2 \cdot 10^{-3}$ S/m, and $\sigma_1^{02} = 0$. In this distribution, one can discern a low-contrast light region in its central part, which corresponds to the position of the cavity.

Figures 11 and 12 show the tomograms of the object-conductivity distributions in the vertical and horizontal sections, which were found by solving Eq. (19) at the level 3% of the simulated random error, which is higher than that in the above-considered examples. A significant enhancement of the requirements imposed on the data accuracy for distributions with more complicated structures is typical of the inverse problems described by the Fredholm equation of the first kind [16]. In the figures, one can see the cavity in the obtained tomographical images. However, significant blurring and smoothing of its shape take place.

Figure 13 presents the results of holographic analysis based on the solution of Eq. (23).

Thus, holographic analysis can be efficient for the objects located at relatively shallow depths and having simply connected inclusions. It allows one to make better judgments about the structure of an object than tomographic images, such as those in Figs. 11 and 12. The problem becomes more complicated for the deeper objects with inclusions, and requires a high accuracy of the input data, which is hardly achievable in practice.

It is important to discuss the issue of the influence of the error in the Born approximation, which was used to derive Eq. (19), on the analysis results. It is known that the Born approximation is fulfilled if the scattered field is low compared with the probing field. This is directly related to the applicability of the method described.

Figure 14 shows an example of calculating the distributions of the electric and magnetic fields for the object having almost the same structure as that shown in Figs. 11–13, i.e., an inhomogeneity having dimensions of $4 \times 4 \times 3$ km and a cavity with dimensions of $2 \times 2 \times 1$ km, which is filled with the material of the external medium. Figure 14*a* presents the calculation results for a medium with a relatively high conductivity $\sigma_0 = 10^{-2}$ S/m at frequencies of 1 and 10 Hz, for which the attenuation factor δ^{-1} was equal to 5.0 and 1.6 km^{-1}, respectively. The inhomogeneity conductivity is assumed equal to the conductivity of the

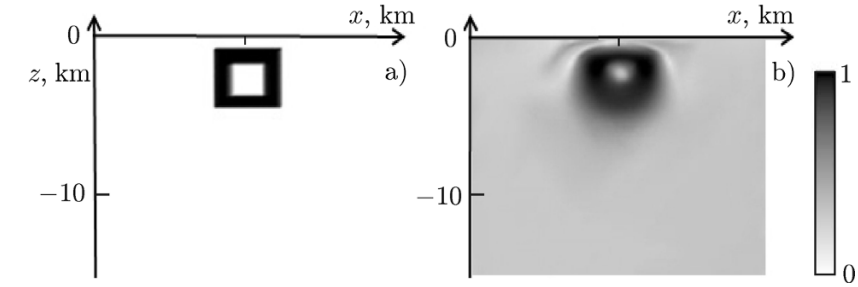

Fig. 11. Simulated distributions of conductivity inhomogeneities (vertical section through the inhomogeneity center) (*a*) and the result of the reconstruction based on the solution of the tomography problem (*b*).

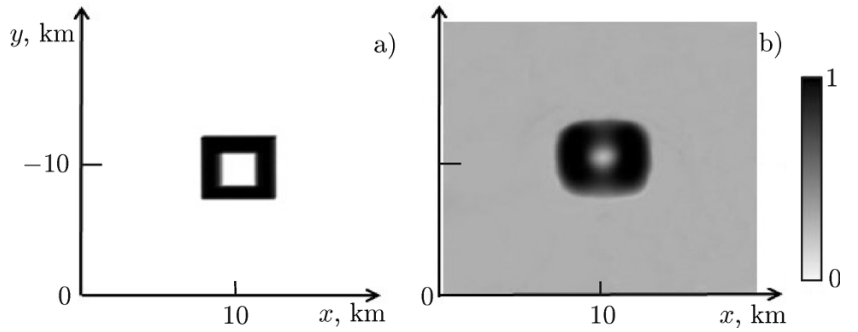

Fig. 12. Simulated distributions of conductivity inhomogeneities (horizontal section through the inhomogeneity center) (*a*) and the result of the reconstruction based on the solution of the tomography problem for $z = -2$ km (*b*).

medium ($\sigma_1 = \sigma_0$). One can see that the fields scattered inside the inhomogeneity excite the external fields weakly, which allows one to use the Born approximation rightfully to solve the problem. Figure 14*b* shows the results for a comparatively weakly conducting medium ($\sigma_0 = 2 \cdot 10^{-4}$ S/m), which, however, contains an object whose conductivity $\sigma_1 = 2 \cdot 10^{-3}$ S/m is an order of magnitude higher. In this case, it is reasonable to use higher frequencies (Fig. 14 shows the results for frequencies of 10 and 100 Hz with attenuation factors of 11.2 and 3.6 km^{-1}, respectively). Despite the smaller value of the medium conductivity, compared with that used in Fig. 14*a*, a noticeable perturbation of the magnetic field occurs inside the object at a frequency of 100 Hz, i.e., a certain error is possible during the calculations in the Born approximation in this case.

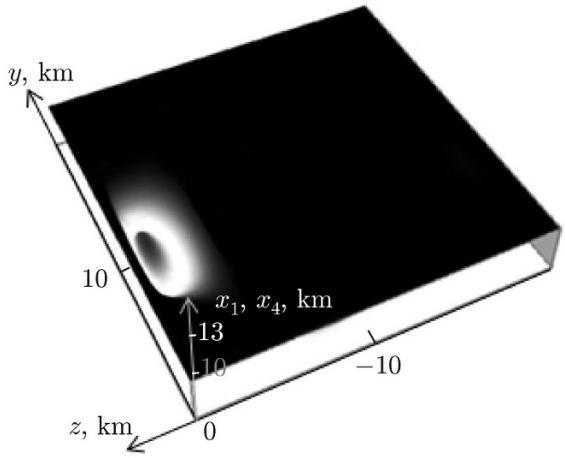

Fig. 13. Holographic image of the inhomogeneity with a cavity. A combination of images of the outer boundary of the object, which is described by the function $x_1(y, z)$, and the inner boundary of the cavity, which is described by the function $x_4(y, z)$.

Despite the above-indicated possibilities of optimization of the measurement parameters, the conductivity of inhomogeneities of the Earth's crust varies in such a wide range that it is not always possible to ensure the fulfillment of the conditions of applicability of the Born approximation. In this connection, a topical task is the development of algorithms that are free of such limitations.

3. SOLUTION BEYOND THE BORN APPROXIMATION

Solution of the initial three-dimensional nonlinear problem on the basis of the dual-regularization method [9–11], which was successfully used for solving a simpler problem in the case of media with a one-dimensional inhomogeneity distribution seems the most consistent approach. However, this approach requires calculations of tens of thousands of three-dimensional field distributions, which are similar to those shown in Fig. 14.

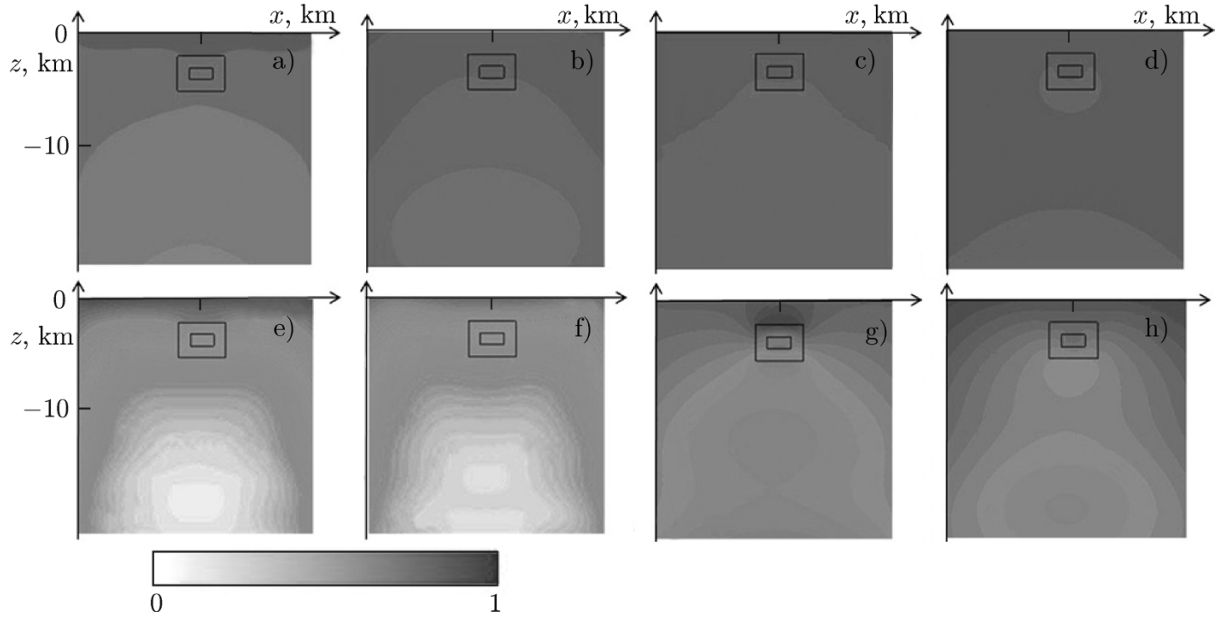

Fig. 14. Normalized (to maximum) amplitudes of the electric (*b*, *d*, *f*, and *h*) and magnetic (*a*, *c*, *e*, and *g*) fields of a plane wave in a medium having the conductivity σ_0 and an object with the conductivity σ_1. Panels *a*, *b*, *e*, and *f* correspond to the case where $\sigma_0 = \sigma_1 = 10^{-2}$ S/m, and panels *c*, *d*, *g*, and *h*, to the case where $\sigma_0 = 2 \cdot 10^{-4}$ S/m and $\sigma_1 = 2 \cdot 10^{-3}$ S/m. The radiation frequency f is equal to 1 Hz (*a* and *b*), 10 Hz (*c*–*f*) and 100 Hz (*g* and *h*).

However, in many cases, one can find the correction to the Born approximation on the basis of the iterative solution of the nonlinear equation, which starts with the distribution of the quantity σ_1^0 found in the Born approximation. The electric field at the nth step of the iterative process has the form

$$E_1(\mathbf{r}) = \int\limits_{V'} \sigma_1^n(\mathbf{r}') \Bigg\{ \iint\limits_{-\infty}^{+\infty} \exp[i\kappa_x (x - x') + i\kappa_y (y - y')] \times [E_{0j}^{(2)}(\mathbf{r}') + E_{1j}^{(2)}(\varepsilon_1^{n-1}, \mathbf{r}') G_{ji}^{21}(\kappa_x, \kappa_y, z, z')\, \mathrm{d}\kappa_x\, \mathrm{d}\kappa_y \Bigg\}\, \mathrm{d}\mathbf{r}', \quad (24)$$

where σ_1^n is the conductivity at the nth iteration, and ε_1^{n-1} is the dielectric permittivity at the $(n-1)$st iteration. If we pass to the spectrum with respect to the transverse coordinates, we obtain the equation

$$E_{1i}(\kappa_x, \kappa_y, z) = 4 \Bigg\{ \int\limits_{z'} \Big\{ \sigma_1^n(\kappa_x - k_x, \kappa_y - k_y, z') E_{0j}^{(2)}(k_x, k_y, z') + \frac{16\pi^2}{\omega} \iint\limits_{-\infty}^{+\infty} \sigma_1^n(\kappa_x - k_x, \kappa_y - k_y, z') \int\limits_{z'} \sigma_1^{n-1}(\kappa_x' - k_x, \kappa_y' - k_y, z'') E_{0k}^{(2)}(k_x, k_y, z'') \times G_{kj}^{22}(\kappa_x', \kappa_y', z', z'')\, \mathrm{d}\kappa_x'\, \mathrm{d}\kappa_y'\, \mathrm{d}z'' G_{ji}^{21}(\kappa_x, \kappa_y, z, z') \Big\}\, \mathrm{d}z'' \Bigg\}, \quad (25)$$

which is one-dimensional only in the first, Born, approximation, when it includes the first term solely. Basically, solving three-dimensional equations (24) and (25) at each step requires a lesser amount of calculations than in the case of application of the methods similar to dual regularization [11], but no absolute convergence of such an iterative procedure is guaranteed in this case. Moreover, even in the case of convergence, the number of steps required to achieve it, can be very great. However, there is still a way allowing one to find the correction to the Born approximation on the basis of Eq. (25), while staying within the framework of

solving the one-dimensional equation. To this end, one should substitute σ_1^{n-1} for σ_1^n into the second term in Eq. (25). Then it becomes a simple correction to the scattered field on the left-hand side of Eq. (25):

$$E_{1i}(\kappa_x,\kappa_y,z)=4\Big\{\int\limits_{z'}\Big[\sigma_1^n(\kappa_x-k_x,\kappa_y-k_y,z')E_{0j}^{(2)}(k_x,k_y,z')$$
$$+\frac{16\pi^2}{\omega}\iint\limits_{-\infty}^{+\infty}\sigma_1^{n-1}(\kappa'_x-k_x,\kappa'_y-k_y,z')\int\limits_{z'}\sigma_1^{n-1}(\kappa'_x-k_x,\kappa'_y-k_y,z'')E_{0k}^{(2)}(k_x,k_y,z'')$$
$$\times G_{kj}^{22}(\kappa'_x,\kappa'_y,z',z'')\,\mathrm{d}\kappa'_x\,\mathrm{d}\kappa'_y\,\mathrm{d}z''\Big]G_{ji}^{21}(\kappa_x,\kappa_y,z,z')\,\mathrm{d}z'\Big\}. \quad (26)$$

Equation (26) is a Fredholm equation of the first kind in the form of Eq. (19) and can be solved in a similar way for each pair of the spectral components. Such a method can yield adequate corrections to the Born approximation without using high-performance computers.

4. CONCLUSIONS

In this work, we have developed methods for computer tomography of distributed conductivity inhomogeneities and for holography (determination of the surface shape) of continuous inhomogeneities and tested these methods by numerical simulation. The methods are based on a mathematically consistent approach, which does not use model representations and parametrization. Most of the results were obtained using the theory of electromagnetic wave scattering in the Born approximation. Approaches allowing one to go beyond this approximation have also been proposed.

The studies were supported by the Russian Foundation for Basic Research (project Nos. 13–07–97028_r_povolzhye and 13–02–12155_ofi_m), Program IV.13 of the Branch of Physical Sciences of the Russian Academy of Sciences, and partially by the Ministry of Education and Science of the Russian Federation (agreement No. 02.V.49.21.0003 of August 27, 2013 between the Ministry of Education and Science of the Russian Federation and N. I. Lobachevsky State University of Nizhny Novgorod).

REFERENCES

1. E. D. Tereshchenko, V. F. Grigor'ev, A. E. Sidorenko, et al., *Geomagn. Aeron.*, **47**, No. 6, 810 (2007).
2. S. V. Polyakov, E. N. Ermakova, A. S. Polyakov, and M. N. Yakunin, *Geomagn. Aeron.*, **42**, No. 2, 223 (2003).
3. A. N. Tikhonov, *Dokl. Akad. Nauk SSSR, New Series*, **73**, No. 2, 295 (1950).
4. A. N. Tikhonov, A. V. Goncharsky, V. V. Stepanov, and A. G. Yagola, *Regularizing Algorithms and a Priory Information* [in Russian], Nauka, Moscow (1983).
5. V. I. Dmitriev, *Ill-Posed Problems in Natural Science* [in Russian], Moscow State Univ. Press, Moscow (1987).
6. K. P. Gaikovich, *Inverse Problems in Physical Diagnostics*, Nova Science Publishers Inc., New York (2004).
7. K. P. Gaikovich, *Phys. Rev. Lett.*, **98**, No. 18, 183902 (2007).
8. K. P. Gaikovich and A. I. Smirnov, *Nizhny Novgorod Univ. Bull.*, No. 2, 73 (2007).
9. K. P. Gaikovich, F. A. Kuterin, A. I. Smirnov, and M. I. Sumin, *Nizhny Novgorod Univ. Bull.*, No. 1, 47 (2009).

10. M. I. Sumin, in: *Advances in Mathematics Research*, Vol. 11, Nova Science Publishers Inc., New York (2010), p. 103.
11. K. P. Gaikovich, P. K. Gaikovich, O. E. Galkin, et al., *Nizhny Novgorod Univ. Bull.*, No. 1(1), 57 (2013).
12. M. S. Zhdanov, *Geophysical Inverse Theory and Regularization Problems*, Elsevier, Amsterdam (2002).
13. M. S. Zhdanov and A. Chernyavskiy, *Inverse Probl.*, **20**, 233 (2004).
14. L. H. Cox and M. S. Zhdanov, *Comm. Comput. Phys.*, **3**, No. 1, 160 (2008).
15. M. S. Zhdanov and E. Tolstaya, *Inverse Probl.*, **20**, 3, 937 (2004).
16. V. V. Spichak, *Izvestiya, Phys. Solid Earth*, **42**, No. 1, 60 (2006).
17. V. V. Spichak and I. V. Popova, *Izvestiya, Phys. Solid Earth*, **34**, No. 1, 33 (1998).
18. K. P. Gaikovich, *Phys. Rev. Lett.*, **98**, 18, 183902 (2007).
19. K. P. Gaikovich and P. K. Gaikovich, *Inverse Probl.*, **26**, 12, 125013 (2010).
20. K. P. Gaikovich, P. K. Gaikovich, Ye. S. Maksimovitch, and V. A. Badeev, *Phys. Rev. Lett.*, **108**, 16, 163902 (2012).
21. K. P. Gaikovich, E. S. Maksimovich, and V. A. Badeev, *Zh. Radioeléktron.*, **6**, 1 (2012).